frontiers | Frontiers in Mechanical Engineering

TYPE Original Research
PUBLISHED 12 January 2026
DOI 10.3389/fmech.2025.1713677

OPEN ACCESS

EDITED BY
Hamid Reza Karimi,
Polytechnic University of Milan, Italy

REVIEWED BY
Zhongjie Li,
Shanghai University, China
Wei Wang,
Zhengzhou University, China

*CORRESPONDENCE
Huiqian Liu,
lhq19820602@163.com

RECEIVED 26 September 2025
REVISED 22 December 2025
ACCEPTED 22 December 2025
PUBLISHED 12 January 2026

CITATION
Sun Y and Liu H (2026) Design and optimization of wireless sensor system for self-powered crawler crane based on piezoelectric energy harvesting.
Front. Mech. Eng. 11:1713677.
doi: 10.3389/fmech.2025.1713677

Design and optimization of wireless sensor system for self-powered crawler crane based on piezoelectric energy harvesting

Yufang Sun[1] and Huiqian Liu[2]*

[1]College of Mechanical and Electrical Engineering Heilongjiang Institute of Technology, Harbin, China, [2]School of New Energy Power and Engineering, Shijiazhuang Institute of Technology, Shijiazhuang, China

Introduction: Crawler cranes are widely used in large–scale infrastructure construction, where structural health monitoring is essential to ensure operational safety. Wireless sensor networks have become a mainstream solution for crane monitoring; however, conventional battery–powered systems suffer from frequent replacement, complex wiring, and limited service life, which restrict long–term deployment.

Methods: To address these issues, a piezoelectric energy harvesting electromechanical coupling model tailored to crawler crane operating conditions is developed. Furthermore, a low–power wireless communication protocol incorporating cluster–head data aggregation and dynamic duty–cycle adjustment is introduced, enabling deep collaboration between energy harvesting, energy storage, and wireless sensing modules.

Results: Simulation results show that within the resonance frequency range of 30–35 Hz, the optimized piezoelectric energy harvesting module achieves a peak output power of 8.0 mW at an acceleration of 0.5 g, representing a 47.5% improvement over the unoptimized configuration. Under the same excitation level, the energy storage capacitor voltage increases to 3.0 V within 25 s. Field deployment experiments involving six sensor nodes demonstrate that the proposed joint optimization scheme attains an energy utilization rate of 81.5%, while extending the average node lifetime to 397.4 h, which is 65.6% longer than that of the unoptimized scheme.

Discussion: This study proposes a "structure–circuit–communication" collaborative optimization framework for complex vibration environments of crawler cranes. The proposed approach enables long-term online monitoring of wireless sensor nodes without batteries and provides a feasible technical pathway for upgrading self-powered Internet of Things systems in large-scale construction machinery.

KEYWORDS

crawler crane, energy management circuit, low power communication, piezoelectric energy harvesting, self-powered, wireless sensor network

1 Background

With the development of engineering machinery and equipment towards large-scale and intelligent direction, crawler cranes are increasingly widely used in infrastructure construction, port loading and unloading, and energy engineering. However, the vibrations, impacts, and load fluctuations generated during equipment operation not only affect structural safety and operational lifespan, but also pose challenges for condition monitoring and fault warning (Baroiu et al., 2023). Wireless sensor networks have gradually become the mainstream choice for real-time monitoring of key parts of cranes. However, traditional wireless sensors rely heavily on battery power supply, which leads to frequent replacement and maintenance, limited lifespan, and complex wiring, limiting their long-term stable application in harsh working conditions (Harle, 2024). In recent years, Energy Harvesting (EH) technology has been considered an effective way to solve the bottleneck of wireless sensor power supply (Zhang et al., 2022). Among them, Piezoelectric Energy Harvesting (PEH) is widely used for energy conversion in mechanical vibration environments due to its high energy density, compact structure, and easy integration (Zou et al., 2021; Bello and Oladipo, 2024). Previous studies have shown that piezoelectric materials can effectively convert low-frequency vibrations into electrical energy, which can be used for powering sensors and operating small electronic devices (Song and Xiong, 2022). However, in complex large cranes, the frequency distribution of vibration signals is wide and the excitation is uneven. How to achieve efficient and stable EH is still an urgent problem to be solved. Meanwhile, the matching optimization between the energy management circuit and the wireless sensor system is insufficient, resulting in a low utilization rate of the collected energy. An optimization scheme for a self-powered wireless sensor system for crawler cranes based on PEH is built, with the aim of proposing improvement ideas in theoretical modeling and circuit optimization.

The innovations of this study are: 1) a PEH electromechanical coupling model was constructed based on the vibration dynamic characteristics of the crawler crane, realizing a deep correspondence between the EH mechanism and the actual working conditions; 2) An adaptive three-stage energy management circuit for unstable vibration environments was proposed, which improves energy utilization through impedance matching and energy storage voltage threshold control; 3) At the system level, the piezoelectric structure, energy management circuit and low-power wireless communication protocol were optimized in a coordinated manner, enabling nodes to maintain stable communication and self-powered operation under high noise and nonlinear vibration conditions. These innovations break through the limitations of previous studies that only focused on a single energy harvesting link or static load conditions, and form a system-level self-powered optimization framework for complex vibration scenarios of engineering machinery.

2 Overview

In recent years, with the increasing demand for long-term online monitoring in engineering equipment, PEH technology based on mechanical vibration has become a hot research direction for self-powered sensor systems. He et al. proposed organic/inorganic composite structures, flexible and stretchable designs, and efficient surface/interface engineering strategies to address the traditional rigid PEH devices being difficult to adapt to flexible and wearable applications, thereby improving the efficiency of mechanical to electrical energy conversion (He and Briscoe, 2024). Tabak et al. improved the efficiency of environmental mechanical vibration collection by introducing a negative Poisson's dilation structure into traditional piezoelectric systems to construct an Auxetic Piezoelectric Energy Harvester (APEH), thereby optimizing the self-powered application of wireless sensors and portable devices (Tabak et al., 2024). Zhang et al. proposed a programmable sharded four stability state function coupled with flexible limit blocks to solve the linear PEH being easily damaged under random broadband excitation. By adjusting the parameters of the segmented four stability state nonlinear PEH potential function, the system's conversion capability was enhanced (Zhang et al., 2024). In response to the low energy density in traditional PEH, Lang et al. developed a piezoelectric material with high transduction coefficient ($d33 \times g33$). By adjusting the composition of piezoelectric materials with different ratios and using phenomenological statistical models to estimate the size of polar nano domains in the sample, it was found that the composition of lead lanthanum zirconate titanate could regulate and awaken ferroelectric domains (Lang et al., 2025).

In the field of condition monitoring for large construction machinery and cranes, energy supply is also a key bottleneck that limits the long-term stable operation of wireless sensors. Song et al. proposed a three-step self-checking cycle estimation, physical model denoising, and edge intelligent fault detection to address the inaccurate operating state and difficulty in extracting fault features of downstream beam pumping units with strong noise. This method achieved high-precision state monitoring and fault diagnosis under limited data quality conditions (Song et al., 2022). Mohsen et al. designed a photovoltaic-thermoelectric hybrid EH powered wearable medical sensor system for long-term healthcare applications. Based on flexible photovoltaic panels, thermoelectric generator modules, Direct Current to Direct Current (DC-DC) boost converters, and two super-capacitors, the system achieved sustainable and long-term monitoring and operation (Mohsen et al., 2021). Peng et al. built a wireless vibration sensor using microelectromechanical systems and ZigBee to address the complex wiring and inconvenient on-site maintenance of traditional wired integrated circuit piezoelectric sensors in transformer vibration monitoring. Compared to parallel operation with wired systems on a 110 kV three-phase transformer, it was found that the waveform period pattern and 50 Hz harmonic energy distribution were consistent with the vibration characteristics of transformers (Peng et al., 2022). Kermani et al. proposed a microgrid architecture that integrated multiple types of energy storage, such as batteries, super-capacitors, and flywheels, and coordinates delay scheduling strategies to address the peak demand surge and rising energy consumption costs caused by impact loads such as large port cranes and cold shore power supply. By uniformly controlling all electrical units such as cranes, refrigerated containers, and office buildings, peak shaving and valley filling as well as renewable energy recovery were achieved, thereby

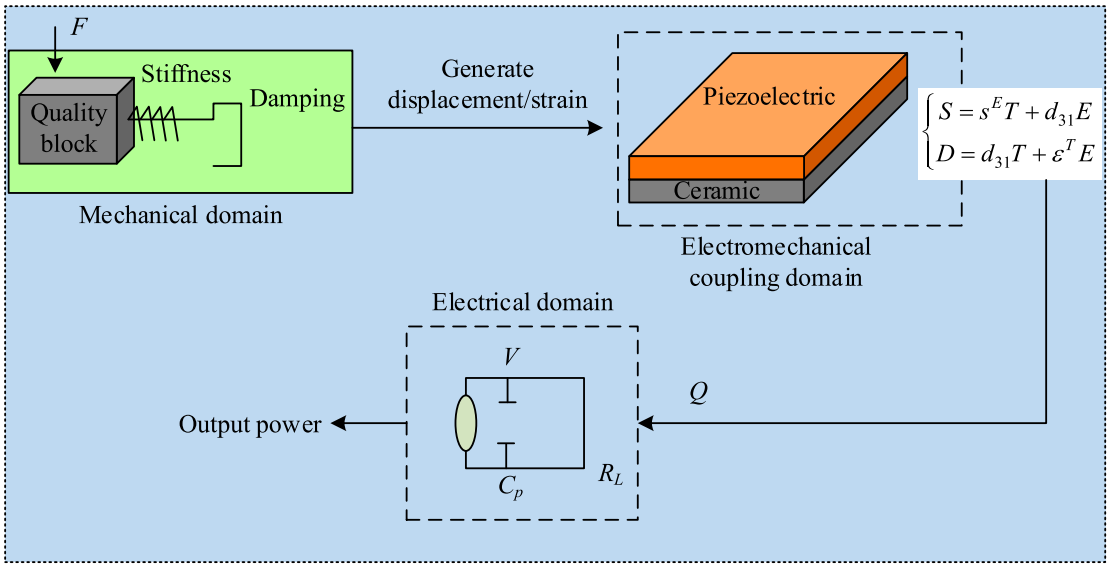

FIGURE 1
Electromechanical equivalent model of PEH.

optimizing the energy structure of the port and reducing operating costs (Kermani et al., 2022).

Overall, existing research has made multiple advances in PEH, from flexible composite structures, nonlinear potential function design to the development of high conversion coefficient piezoelectric materials, all of which have played a positive role in improving the efficiency of mechanical and electrical energy conversion. In the field of engineering machinery and crane monitoring, scholars have also tried various optimization methods to alleviate the insufficient energy supply. However, most EH devices have limited efficiency under low-frequency and broadband vibrations, making it difficult to adapt to complex working conditions of cranes. Insufficient collaborative optimization between energy management circuits and wireless sensor nodes results in low energy utilization efficiency. Therefore, an optimization method for a self-powered wireless sensor system for crawler cranes based on PEH is proposed, aiming to achieve long-term self-powered operation of sensor nodes by establishing a PEH model under crane operating conditions, designing efficient energy management circuits, and deeply integrating with low-power wireless sensor networks. The main innovations of the research are as follows. A PEH model based on the actual vibration characteristics of the crane is established to adapt to complex working conditions. A collaborative optimization method for circuit and sensor systems is proposed to effectively improve the utilization of collected energy.

3 Research methodology

Firstly, a complex electromechanical coupling model for crawler crane vibration is established to elucidate the energy conversion mechanism under low-frequency broadband random excitation. Secondly, a three-level energy management circuit of "rectification-energy storage-DC-DC boost" is designed and deeply integrated with low-power wireless sensors to coordinately optimize structure-circuit-communication.

3.1 Piezoelectric energy harvesting and circuit design

PEH technology relies on the electromechanical coupling effect of piezoelectric materials under vibration or stress, which essentially converts mechanical energy into electrical energy and stores, providing a stable self-powered power source for wireless sensor nodes (Amer et al., 2025). In response to the low-frequency and broadband vibration characteristics of crawler cranes during operation, the study first establishes an electromechanical equivalent model of piezoelectric transducers, and then optimizes the design based on circuit topology. The piezoelectric transducer generates strain and charge under external force, and its constitutive relationship is shown in Equation 1.

$$\begin{cases} S = s^E T + d_{31} E \\ D = d_{31} T + \varepsilon^T E \end{cases} \tag{1}$$

In Equation 1, S signifies the strain. D signifies potential shift. T signifies the stress. E signifies the electric field strength. s^E represents the elastic flexibility constant. d_{31} signifies the piezoelectric strain coefficient. ε^T represents the dielectric constant. In equivalent circuit modeling, piezoelectric transducers are usually abstracted as a voltage source in parallel with a capacitor, and their mechanism of action is shown in Figure 1.

In Figure 1, the mechanical vibration input on the left is simplified as an external excitation force F, which generates strain through a piezoelectric element and converts it into a charge Q. In the electrical equivalent circuit, this process is equivalent to an AC voltage source V connected in parallel with a capacitor C_p, and the output terminal is connected to a load resistor R_L. This model can directly reflect the conversion

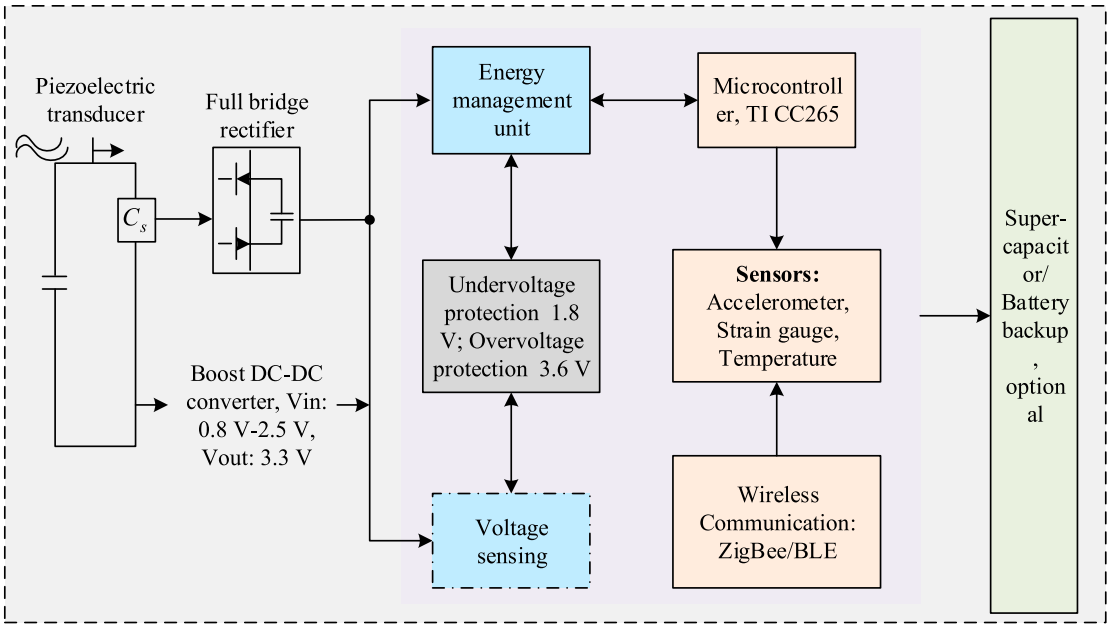

FIGURE 2
PEH circuit topology.

relationship between external mechanical energy input and electrical output power, and lays a theoretical foundation for impedance matching and circuit optimization. When the piezoelectric element is subjected to an excitation force F, the amount of charge generated and the corresponding mathematical expression for the output voltage are shown in Equation 2.

$$\begin{cases} Q = d_{31}FA \\ V = \dfrac{Q}{C_p} \end{cases} \tag{2}$$

In Equation 2, A signifies the effective area of the piezoelectric sheet. The geometric parameters and dielectric constant of piezoelectric sheets directly determine their electrical output characteristics (Meisak et al., 2024). Therefore, the study further considers the load effect and obtains the output power expression, as shown in Equation 3.

$$P = \frac{V^2}{R_L} \cdot \frac{R_L}{R_L + 1/\left(j\omega C_p\right)} \tag{3}$$

In Equation 3, P represents the output power of PEH. j represents the imaginary unit. ω represents the angular frequency of vibration. When the load impedance matches the equivalent impedance of the piezoelectric element, the system output power reaches its maximum value. However, the output voltage of the piezoelectric element is an AC signal with limited amplitude. Therefore, rectification, energy storage, and voltage regulation are necessary to stably drive the sensor node. The research adopts a three-stage topology structure of full wave rectification-energy storage capacitor-DC-DC boost converter to optimize the EH circuit. The specific principle is shown in Figure 2.

In Figure 2, the output AC voltage of the piezoelectric element first passes through a rectifier bridge, converting the bidirectional AC waveform into unidirectional pulsating DC. Subsequently, the voltage fluctuation is smoothed through the energy storage capacitor C_s, and charge is accumulated. A boost DC-DC converter is configured at the output end to steadily increase the energy storage voltage to the operating voltage range of the wireless sensor (1.8 V–3.3 V). The entire process ensures that the vibration energy can be fully collected and utilized, and provides stable power supply for the sensor. The rectified DC voltage V_{dc} is shown in Equation 4.

$$V_{dc} = \frac{2}{\pi}V_{ac} - 2V_d \tag{4}$$

In Equation 4, V_{ac} represents the peak AC voltage of the piezoelectric element. V_d represents the voltage drop across the diode. The voltage variation of the energy storage capacitor during the charging process is shown in Equation 5.

$$V_c(t) = V_{dc}\left(1 - e^{-\frac{t}{R_L C_s}}\right) \tag{5}$$

The capacitor gradually approaches a stable voltage over a long period of time, and its dynamic characteristics directly affect the starting and power supply capabilities of the sensor node. Therefore, the energy utilization rate of the final system is defined in Equation 6.

$$\eta = \frac{\int V_{out}(t) I_{load}(t) dt}{\int V_P(t) I_P(t) dt} \tag{6}$$

In Equation 6, η represents the energy utilization rate of the system, and the higher its value, the better the degree of circuit optimization. $V_{out}(t)$ represents the instantaneous voltage at the load end. $I_{load}(t)$ signifies the current at the load end. $V_p(t)$ signifies the instantaneous voltage at the output end of the piezoelectric transducer. $I_p(t)$ signifies the output current of

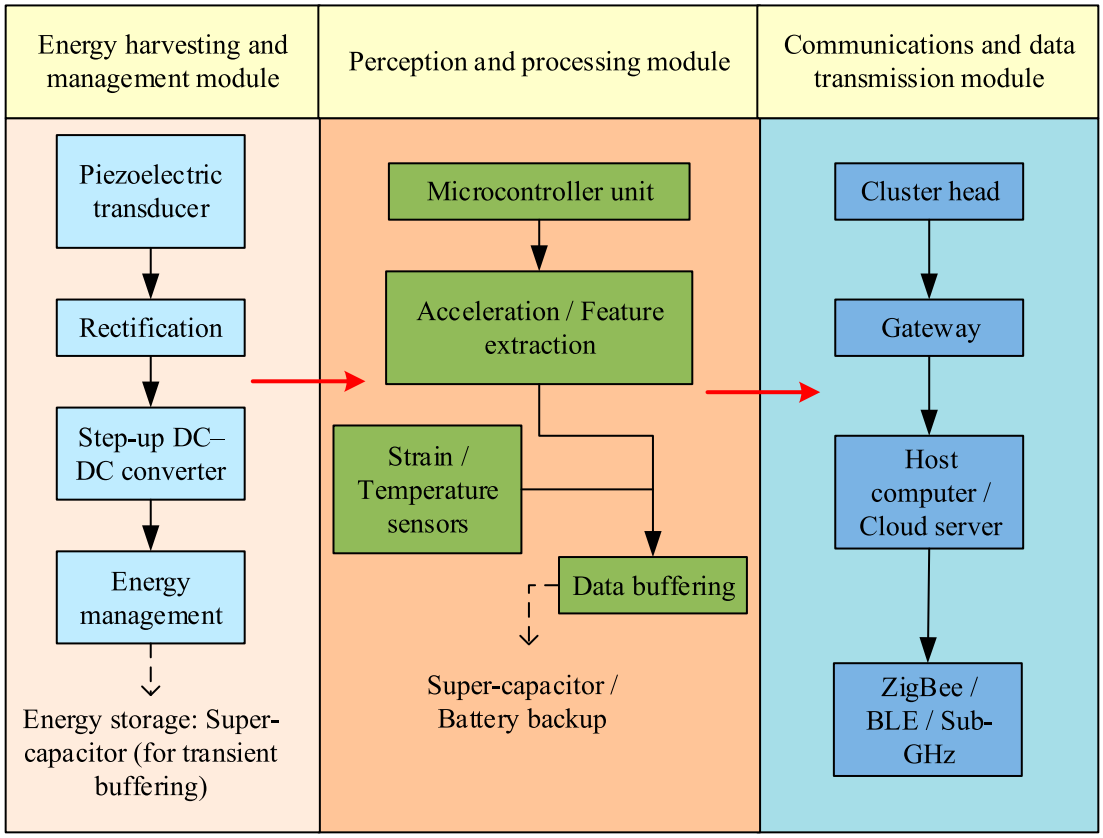

FIGURE 3
Overall architecture of the wireless sensor system.

the piezoelectric element. $\int V_{out}(t)I_{load}(t)dt$ represents the effective energy obtained by the load within a certain period of time. $\int V_{out}(t)I_{load}(t)dt$ represents the total energy converted by the piezoelectric transducer from vibration within a certain period of time. The instantaneous voltage was synchronously acquired using a National Instruments Data Acquisition (NI-DAQ) system at a sampling frequency of 10 kHz. The output current was measured by connecting a precision sampling resistor (0.1 Ω) in series with the load terminal of the power management circuit. The sampled voltage signal was input differentially to the NI-DAQ data acquisition card and recorded synchronously.

3.2 Wireless sensor system integration

In complex working conditions of crawler cranes, vibration signals come from a wide range of sources and have a large frequency distribution span. Therefore, relying solely on PEH circuits is difficult to ensure long-term stable power supply. To achieve online monitoring of key structural components, the PEH circuit is deeply integrated with wireless sensor nodes to form a self-powered, low-power, and multi-node collaborative monitoring system. This system not only enables effective energy collection and scheduling, but also optimizes sensor sampling, data processing, and wireless communication to ensure efficient and reliable state perception and data transmission under limited energy supply conditions. The system summary architecture is shown in Figure 3.

From Figure 3, the self-powered wireless sensor system has an energy collection and management module, a perception and processing module, and a communication and data transmission module. Among them, the energy collection and management module converts vibration mechanical energy into electrical energy through a piezoelectric energy collector, and supplies power to the nodes through rectification, energy storage, and voltage boosting and stabilization processes. The perception and processing module is equipped with acceleration sensors, strain gauges, and inclination sensors to monitor the dynamic response of key parts of the crane, and preprocesses and extracts features through a microprocessor unit. The communication and data transmission module adopts low-power wireless communication protocol to achieve data exchange between multiple nodes and remote communication with the gateway. Based on the system architecture, the study first conducts node energy management and power consumption modeling. The energy consumption of wireless sensor nodes mainly comes from three parts: sampling, processing, and communication. Therefore, the total energy consumption can be shown in Equation 7.

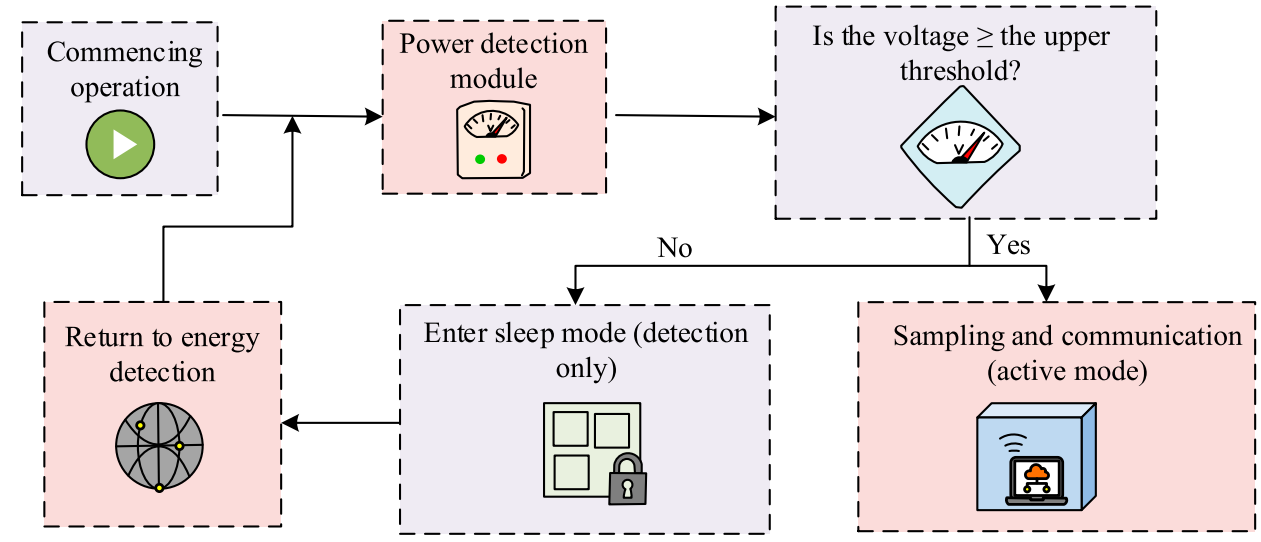

FIGURE 4
Energy management process for wireless sensor nodes.

$$\begin{cases} E_{node} = E_{sense} + E_{proc} + E_{comm} \\ E_{sense} = P_{sense} \cdot t_{sense} \\ E_{proc} = P_{proc} \cdot t_{proc} \\ E_{comm} = P_{tx} \cdot t_{tx} + P_{rx} \cdot t_{rx} \end{cases} \quad (7)$$

In Equation 7, E_{node} signifies the total energy consumption. E_{sense} signifies the energy consumption of the sensor during the sampling phase. E_{proc} signifies the communication energy consumption of the processor during the feature extraction and data packaging stages. E_{comm} signifies the communication energy consumption of the node during the sending and receiving phases. P_{sense} signifies the power consumption during the sensor sampling phase. t_{sense} represents the duration of sensor sampling. P_{proc} represents data processing power consumption. t_{proc} represents the duration of the processing phase. P_{tx} and P_{rx} represent the power consumption of nodes during wireless transmission and reception, respectively. t_{tx} and t_{rx} respectively represent the time for nodes to transmit and receive data within one cycle. To ensure energy self-sufficiency of nodes, it is necessary to meet the conditions of energy supply and demand balance, as shown in Equation 8.

$$E_{harvested} \geq E_{node} \quad (8)$$

In Equation 8, $E_{harvested}$ represents the total energy collected by the piezoelectric system during one working cycle. If the energy is insufficient, the node must reduce the duty cycle or enter sleep mode. Therefore, the study proposes an energy management mechanism based on the voltage of energy storage capacitors. When the voltage exceeds the upper threshold V_{th1}, the node enters active mode and performs acquisition and communication tasks. When the voltage is below the lower threshold V_{th2}, the node enters sleep mode, retaining only the clock circuit and energy detection module. The specific process is shown in Figure 4.

In Figure 4, when the energy storage voltage is high enough, the node executes the complete data acquisition and communication process When the voltage is insufficient, the node automatically enters low-power sleep mode and restarts after energy is restored. This mechanism can ensure the stable operation of the system under limited energy conditions. On this basis, the low-power communication protocol and network topology of the system are optimized. In multi-node monitoring scenarios, communication energy consumption typically accounts for over 50% of the total energy consumption of nodes (Kundu et al., 2025). Therefore, reducing communication energy consumption is the key to system design. The communication energy consumption is presented in Equation 9.

$$E_{comm} = N_{pkt} \cdot (E_{tx} + E_{rx}) \quad (9)$$

In Equation 9, N_{pkt} represents the number of data packets transmitted in each cycle. $E_{tx} = P_{tx} \cdot t_{tx}$ signifies the energy consumption of sending a single data packet. $E_{rx} = P_{rx} \cdot t_{rx}$ signifies the energy consumption of receiving a single data packet. To reduce redundant communication, the Cluster Head (CH) aggregation mechanism is introduced. The CH node compresses and summarizes the data within the cluster, and then uploads it uniformly to the gateway. The CH is selected based on a weighting factor of node remaining energy and link quality, as shown in Equation 10.

$$W_i = \alpha \frac{E_i}{E_{\max}} + \beta \frac{LQ_i}{LQ_{\max}} \quad (10)$$

In Equation 10, α and β represent weight factors, satisfying $\alpha + \beta = 1$ (Gupta et al., 2024). W_i represents the comprehensive weight of node i. E_i signifies the remaining energy of node i. $E_{\max}$ signifies the maximum remaining energy of nodes in the network. LQ_i represents the link quality of node i. $LQ_{\max}$ represents the best link quality in the network. In addition, to further reduce energy consumption, the node adopts Duty Cycling (DC) control. The specific mathematical expression is shown in Equation 11.

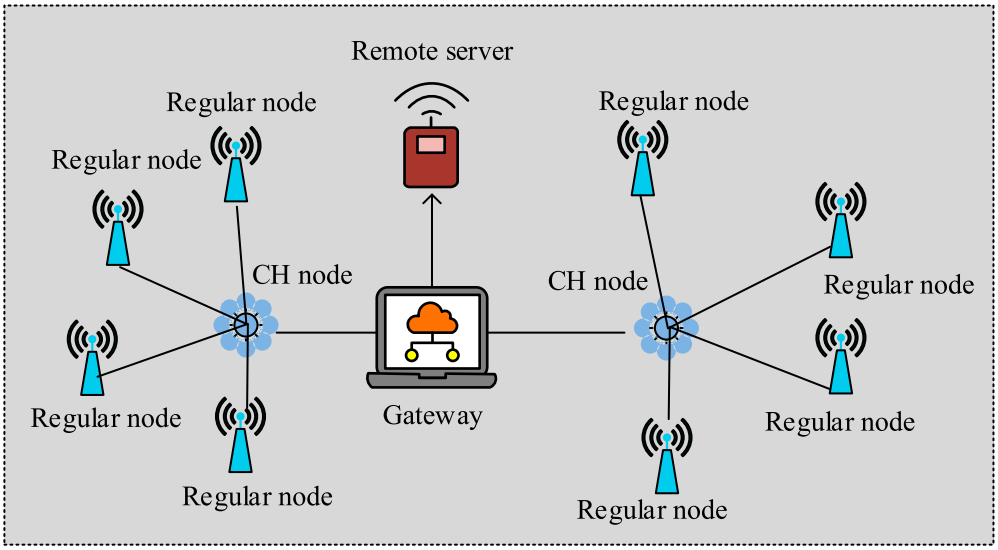

FIGURE 5
Wireless sensor network communication topology.

$$DC = \frac{t_{active}}{t_{active} + t_{sleep}} \tag{11}$$

In Equation 11, t_{active} represents the duration of node activity. t_{sleep} represents the duration of sleep. Considering the high-vibration and nonuniform energy environment of the crane, the study introduces vibration- and energy-aware weighting factors into CH selection and employs a voltage-threshold-based adaptive adjustment function in DC control to accommodate energy fluctuations, achieving stable communication and balanced energy utilization. By dynamically adjusting the DC, the system's operational lifetime can be extended while maintaining data reliability. The network communication topology of wireless sensors is shown in Figure 5.

In the topology shown in Figure 5, the ordinary nodes first transmit the locally collected vibration and strain data to the CH node. After receiving it, the CH fuses, compresses, and redundantly removes the data, and uploads it uniformly to the gateway or upper computer. Compared with the traditional node direct transmission method, the CH mechanism not only reduces data redundancy and energy consumption caused by frequent communication between nodes, but also balances the energy consumption of each node through reasonable CH election, avoiding network partitioning caused by premature energy depletion of some nodes. This topology can improve transmission efficiency, reduce power consumption, and enhance network robustness, providing stable support for long-term online monitoring of multiple nodes under complex working conditions of cranes.

4 Results and discussion

Firstly, the output characteristics of the PEH module are tested under three excitation levels of 5 Hz–80 Hz and 0.1 g–0.5 g on a vibration table. Secondly, energy utilization efficiency, node lifespan, and network robustness are evaluated in a 6-node networking environment on-site, verifying the effectiveness of the system's long-term self-powered operation.

4.1 Experimental setup

To verify the feasibility and superiority of the self-powered wireless sensor system for crawler cranes, an experimental platform is built and tested under typical working conditions. The experimental platform consists of a PEH module, an energy management circuit, wireless sensor nodes, and a data acquisition system. The specific details are shown in Figure 6.

Table 1 presents the experimental hardware environment configuration.

Table 1 shows the power consumption characteristics of the CC2650 chip in different operating modes as follows: power consumption is approximately 1.1 mW (330 μA@3.3 V) in idle listening mode, approximately 4.2 mW (1.27 mA@3.3 V) in data acquisition and processing mode, and approximately 33 mW (10 mA@3.3 V) in wireless transmission mode. Based on the parameter settings shown in Table 1, to simulate the vibration characteristics of a crawler crane during actual operation, the experiment takes an electromagnetic vibration table to load excitation signals of different frequencies and amplitudes. The excitation frequency range is set to 5 Hz–80 Hz, covering the main vibration frequency bands of the crawler crane during travel and lifting. The excitation amplitude is divided into three levels: low intensity (0.1 g), medium intensity (0.3 g), and high intensity (0.5 g), corresponding to light load, rated load, and heavy load conditions, respectively. In addition, six wireless sensor nodes are deployed, which are installed at key parts such as the base of the boom, the middle section of the boom, the lifting mechanism, the slewing support, the track frame, and the engine base of the crawler crane. Each node is

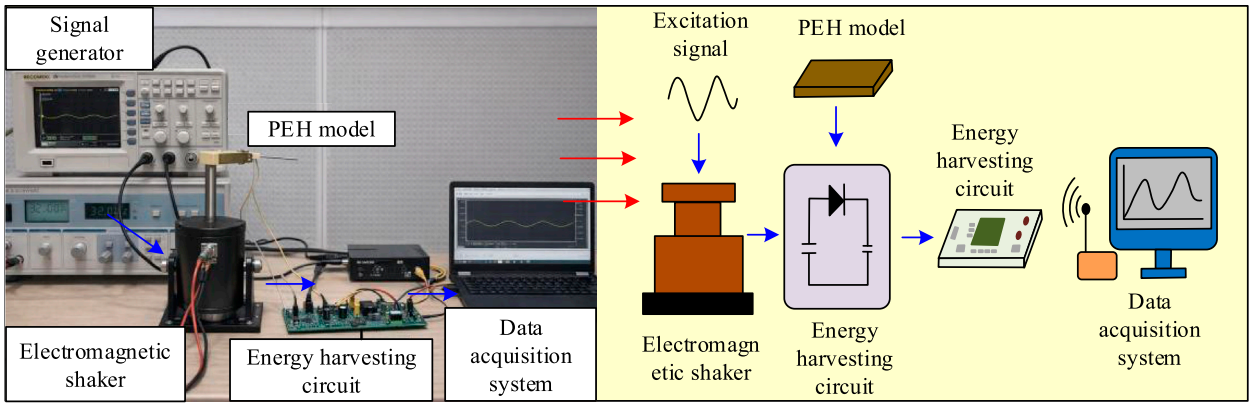

FIGURE 6
Schematic diagram of experimental platform setup and equipment connection (Image source: Photo taken by the author).

TABLE 1 Experimental hardware and parameter configuration.

Category	Configuration parameters
Piezoelectric transducer	PZT-5H, d_{31} = -274 pC/N, C_p = -120 nF
Circuit module	Full-wave rectifier bridge +100 μF storage capacitor + DC-DC converter
Sensor node	CC2650 chip, three-axis accelerometer, strain gauge, temperature sensor
Operating voltage	1.8 V–3.6 V
Data acquisition system	NI-DAQ + MATLAB/Simulink

equipped with a PEH module to achieve self-powered operation. The EH module is arranged closely to the metal structure, fully utilizing the vibration energy of the structure. The wireless communication module transmits data to the central gateway through clustering mechanism. In addition, to ensure the stability of the EH and management process, the three-stage energy management circuit consists of three parts: rectification, energy storage, and boost regulation. The rectification section uses a 1N5819 Schottky diode bridge full-wave rectifier, the energy storage section uses a 100 μF tantalum capacitor (with a withstand voltage of 10 V), and the boost regulation section uses a TI TPS61070 DC-DC boost chip, with the output voltage stabilized at 3.3V ± 0.05 V. Table 2 shows typical vibration measurement results for the six nodes.

Table 2 shows that the main vibration energy at the six nodes is mostly concentrated in the 10–50 Hz range. The peak acceleration at the boom root and slewing platform is approximately 0.20–0.40 g, while the peak acceleration at the engine mount and chassis is mostly in the 0.05–0.15 g range. This indicates that the vibration amplitude at different locations varies with the structural stress state, but its typical excitation range is basically consistent with the 5–80 Hz excitation frequency band and 0.1–0.5 g excitation amplitude set for the experimental platform, representing the structural vibration characteristics under common operating scenarios of crawler cranes.

4.2 Comprehensive analysis of energy harvesting and communication performance

To ensure that the vibration table test matches the actual working conditions of the crawler crane, the study first deployed triaxial accelerometers at key stress-bearing components such as the crane boom root, middle segment, slewing platform, and track frame. The sampling frequency was set to 1,000 Hz, and vibration data was continuously recorded for 300 s under each working condition. A representative 10 s signal segment was then extracted for time-domain analysis. The time-domain waveforms

TABLE 2 Typical vibration measurement results of six nodes deployed on site.

Node location	Dominant frequency (Hz)	Peak acceleration (g)	Operation scenario
Boom base	22–35	0.20–0.40	Slewing/lifting
Boom mid	18–30	0.15–0.30	Lifting
Slewing platform	20–40	0.20–0.40	Slewing
Engine base	10–20	0.05–0.15	Traveling
Chassis frame	10–18	0.05–0.12	Traveling
Track support	10–18	0.06–0.14	Traveling

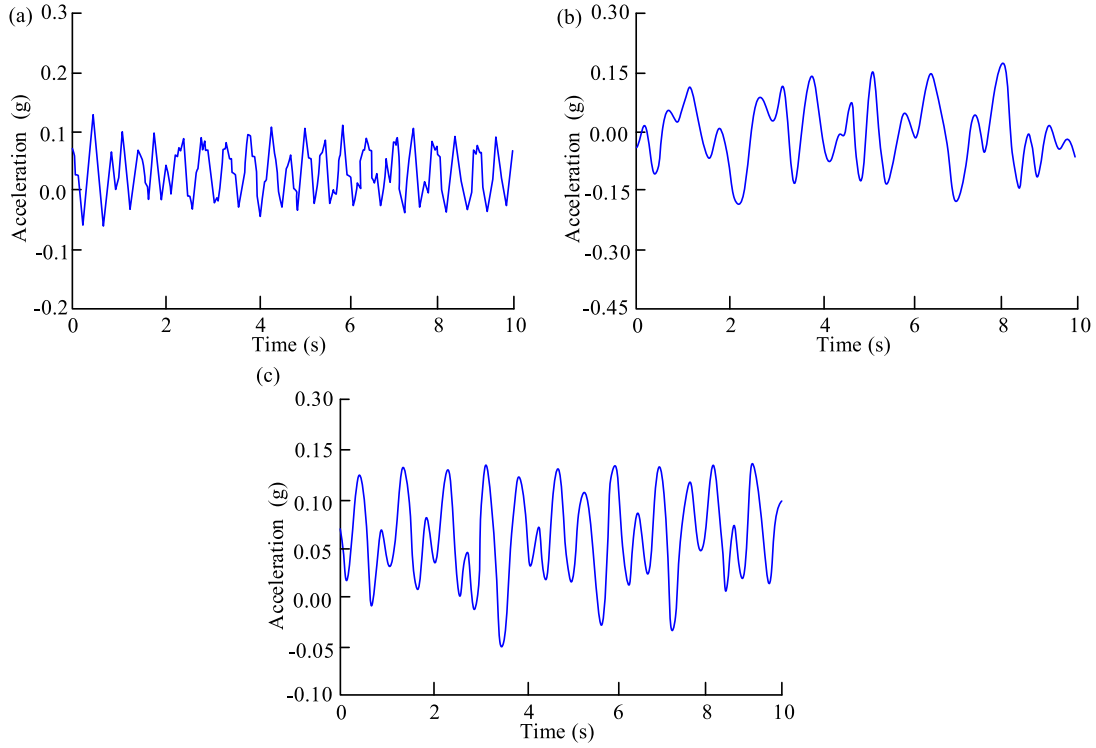

FIGURE 7
Time-domain acceleration signals of crawler cranes under three typical working conditions. **(a)** Walking condition. **(b)** Slewing condition. **(c)** Lifting conditions.

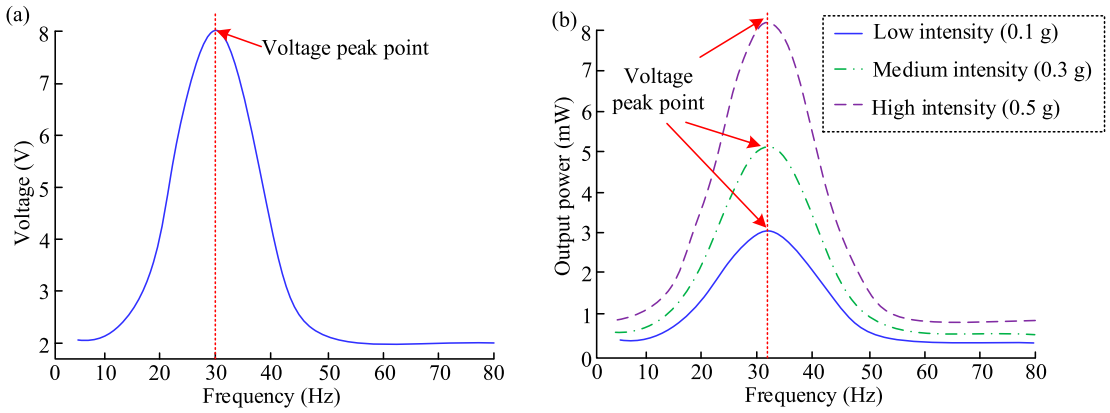

FIGURE 8
PEH performance test results. **(a)** Output voltage versus frequency curve. **(b)** Output power versus frequency curve.

for the three working conditions—traveling, slewing, and rated lifting—are shown in Figure 7.

As shown in Figure 7a, the acceleration mainly fluctuates within the range of ±0.15 g during the walking operation, exhibiting a continuous quasi-periodic signal with a relatively small amplitude. Figure 7b shows that the vibration amplitude increases significantly during the slewing operation. Figure 7c indicates that the vibration signal exhibits a more pronounced periodic component during the hoisting operation, accompanied by certain amplitude fluctuations. This is mainly due to the significant influence of load changes on the hoisting mechanism. To comprehensively verify the effectiveness of the proposed PEH and self-powered wireless sensor system under the working conditions of crawler cranes, a comprehensive analysis is conducted from three aspects: EH characteristics, circuit output stability, and wireless communication performance. The output voltage and power characteristics of the PEH are tested at

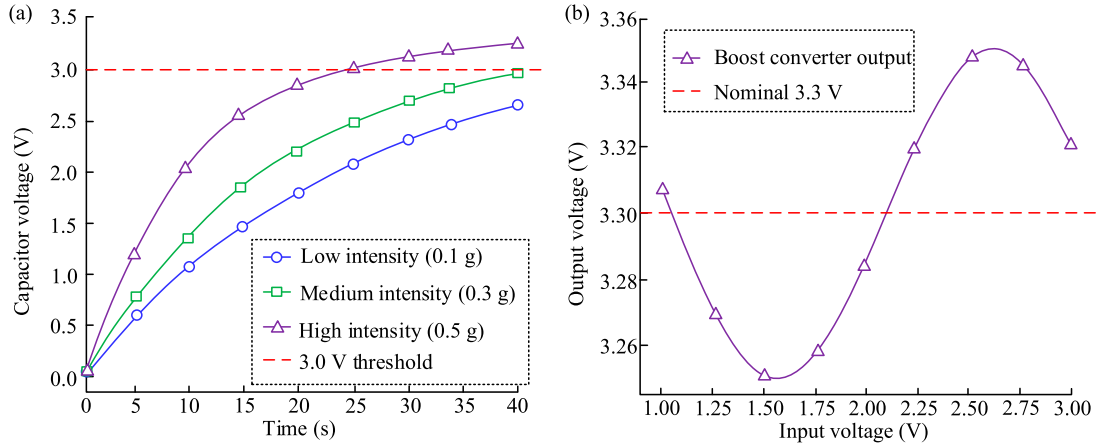

FIGURE 9
Performance analysis results of the energy management circuit. **(a)** Charging curve for energy storage capacitors. **(b)** Voltage regulation characteristics of the boost circuit.

different frequencies and excitation intensities, and the results are shown in Figure 8.

From Figure 8a, the output voltage of the piezoelectric transducer exhibited a clear peak characteristic with frequency variation. At a low frequency of 10 Hz, the open circuit voltage was only about 2.1 V, while it reached a maximum of 8.0 V around 30 Hz. As the frequency continued to increase, the voltage gradually decayed to around 2.2 V. This indicates that the transducer can generate higher voltage output under excitation conditions close to its natural frequency, due to the resonance effect that significantly amplifies the strain response of the piezoelectric sheet. Figure 8b shows the power output curves under different excitation intensities. At 32 Hz, the peak power corresponding to low intensity (0.1 g) was 2.9 mW, medium intensity (0.3 g) was 5.2 mW, and high intensity (0.5 g) reached 8.0 mW. Compared with low intensity, medium and high intensity were significantly improved. This indicates that power output not only depends on excitation frequency matching, but also increases approximately linearly with the amplitude of external vibrations. The reason is that when the excitation acceleration increases, the piezoelectric plate undergoes more obvious force deformation, resulting in more charge accumulation and improved energy conversion efficiency. It is worth noting that the vibration of actual crawler cranes contains certain random components and structural nonlinearities, which may cause amplitude dependence and frequency drift behavior. Since typical lifting and slewing conditions have narrow-band vibration characteristics, and the structure used in this paper has a high mechanical quality factor, the nonlinear effects are relatively weak within the studied vibration range. The performance analysis results of the energy management circuit are shown in Figure 9.

From Figure 9a, the charging speed of the energy storage capacitor varied under different excitation conditions. When the excitation intensity was 0.5 g, the capacitor voltage could be charged to 3.0 V within 25 s, while it took about 40 s at medium intensity (0.3 g) and longer at low intensity (0.1 g). Compared with low intensity, the charging efficiency of medium and high intensity was significantly improved. Figure 9b shows the voltage regulation characteristics of the DC-DC boost circuit at different input voltages. When the input voltage fluctuated within the range of 1.2 V–2.8 V, the output voltage remained stable at 3.3 V ± 0.05 V, and the voltage fluctuation amplitude did not exceed 1.5%. The sensor communication performance and energy consumption based on PEH are shown in Figure 10.

According to Figure 10a, the system communication success rate remained above 90% within 0 m–40 m. When the transmission distance increased to 60 m, the success rate decreased to 89.5%, with a decrease of 3.14% compared to 20 m. This indicates that wireless communication reliability between nodes is high within the typical operating radius of the crane, but signal attenuation and multi-path interference effects are significantly enhanced in long-distance transmission exceeding 60 m. This is likely because the steel structure of the crane, such as its boom or chassis, can reflect and shield wireless signals, leading to multipath propagation and fading. When the communication distance exceeds 60 m, the signal needs to pass through or diffract around metal components, causing a decrease in strength and an increase in the bit error rate, thus slightly reducing the communication success rate. The system effectively mitigates this impact by using a received signal strength indication threshold for retransmission and optimizing node location. Figure 10b shows the impact of CH mechanism on energy consumption. When the CH mechanism was not used, the relative energy consumption benchmark of network nodes was 100%. After adopting CH polymerization, the energy consumption decreased to 58.4%.

4.3 Multi-objective optimization and comparative analysis

In complex working conditions of crawler cranes, the system not only needs to ensure energy collection efficiency, but also needs to consider communication performance, node lifespan, and network stability. Therefore, the study first analyzes the multi-objective optimization performance of the system, as shown in Figure 11.

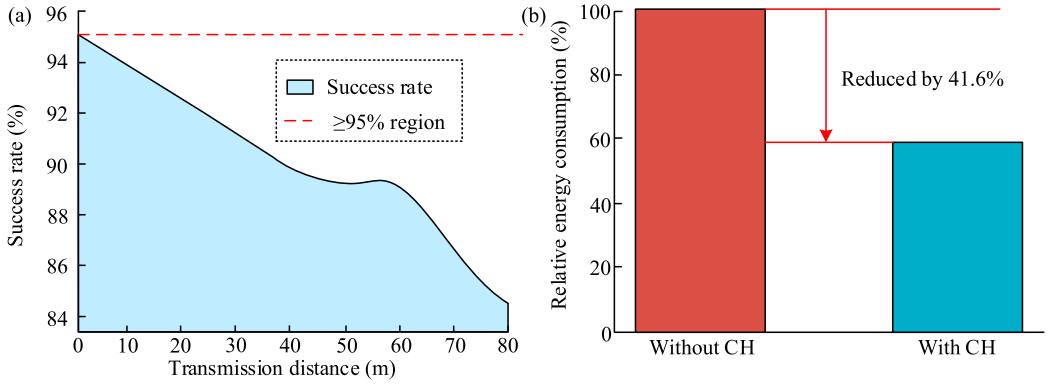

FIGURE 10
Comparison of wireless communication performance and energy consumption. **(a)** Communication success rate versus distance curve. **(b)** Energy consumption comparison with CH mechanism enabled/disabled.

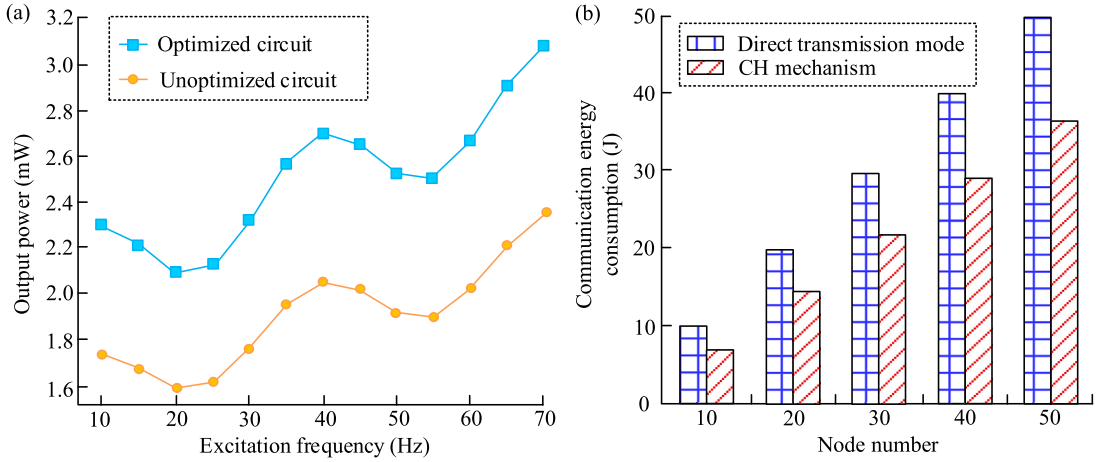

FIGURE 11
Comparison of system multi-objective optimization effects. **(a)** EH efficiency comparison curve. **(b)** Communication energy consumption comparison.

From Figure 11a, within the excitation frequency range of 10 Hz–70 Hz, the output power of the optimized circuit was always higher than that of the unoptimized circuit. In the resonance frequency range of 30 Hz–35 Hz, the peak power of the optimized circuit reached 2.7 mW, with an increase of 47.5% compared to the unoptimized circuit. In the non-resonant frequency range, the optimized circuit also exhibited smoother power output, indicating that its impedance matching and energy management design effectively improved energy loss. From Figure 11b, the total communication energy consumption of the direct transmission mode increased approximately linearly with the number of nodes and was higher than that of the CH mechanism at different numbers of nodes. When the number of nodes was 50, the CH mechanism reduced communication consumption by 29.2% compared to direct transmission mode. This indicates that the CH mechanism effectively reduces redundant transmission through intra cluster data fusion and compression. On this basis, the study further analyzes the node lifetime and network robustness under different optimization strategies, as shown in Figure 12.

From Figure 12a, under the unoptimized scheme, the average lifespan of nodes remained at 240.0 h. However, both circuit optimization and communication optimization could extend the lifespan, increasing it to 311.5 h and 330.7 h, respectively. The joint optimization scheme had the most significant effect, at average lifespan of 397.4 h, with an increase of 65.6% compared to the unoptimized scheme. This indicates that the synergistic effect of EH and communication optimization can effectively alleviate energy consumption pressure and extend the network lifecycle. Figure 12b reflects the proportion of failed nodes over time under different strategies. The study defines node failure as a node failing to report data for 10 consecutive communication cycles, or a state where the energy storage voltage remains below 2.2 V and cannot automatically recover operation. After running for 500 h, the failure rate of unoptimized solutions exceeded 70%, leading to

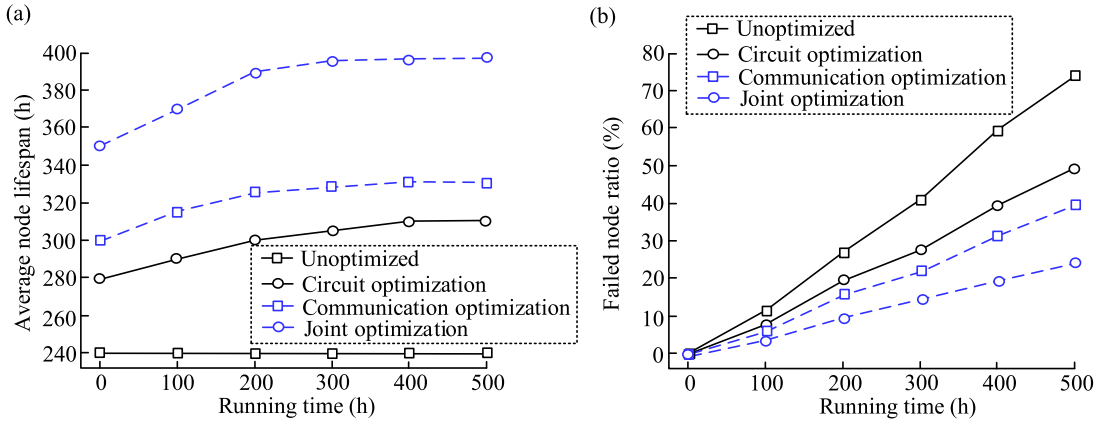

FIGURE 12
Node lifespan and network robustness analysis. **(a)** Comparison of average node liftspan. **(b)** Changes in the proportion of failed nodes.

TABLE 3 Comprehensive performance comparison of multi-objective optimization.

Optimization strategy	Energy utilization (%)	Network throughput (kbps)	Average latency (ms)	Packet loss rate (%)
Unoptimized	62.5	85	92.3	12.4
Circuit optimization	78.3	88.7	84.6	9.7
Communication optimization	74.2	95.4	70.8	6.8
Joint optimization	81.5	102.6	65.3	4.5

widespread network paralysis. The failure rate of the joint optimization scheme was only 25.2%, demonstrating better network robustness. The comprehensive performance analysis results of multi-objective optimization are presented in Table 3.

From Table 3, different optimization strategies have differences in energy utilization, network communication quality, and system stability. Compared with the other three strategies, the joint optimization had the best effect, reaching 81.5%, indicating that it could more efficiently convert piezoelectric energy into usable electrical energy. Under the unoptimized scheme, the system throughput was 85.0 kbps and the average latency was 92.3 ms. The joint optimization scheme improved throughput to 102.6 kbps and reduced latency to 65.3 ms, indicating that joint optimization can simultaneously enhance data transmission capability and real-time performance. Combined with packet loss rate, the joint optimization scheme has superiority in energy utilization and communication performance. This strategy not only improves EH efficiency, but also ensures wireless communication quality and robust operation capability.

5 Discussion

The PEH electromechanical coupling model constructed in this study is based on linear constitutive relations and can accurately describe the motor switching law under low-to-medium amplitude vibration. Experimental results show that the proposed collaborative optimization system achieves stable EH and wireless communication under typical vibration conditions of crawler cranes. The PEH module reaches its peak output power in the 20–50 Hz main frequency range, verifying the effective characterization of vibration energy distribution characteristics by the constructed electromechanical coupling model. The three-stage energy management circuit improves energy utilization through adaptive impedance matching and energy storage voltage threshold adjustment, enabling the node's average operating life to reach 397.4 h. This result demonstrates that the collaborative mechanism between energy management and communication scheduling effectively mitigates the uncertainty caused by energy fluctuations, enabling the system to achieve long-term stable operation without external power supply.

Compared with existing research or commercial energy harvesting solutions (such as LTC3588, BQ25570, etc.), the circuit and protocol optimizations in this study exhibit better robustness and adaptability in dealing with unstable mechanical vibration and high-noise communication environments. The PEH unit is directly attached to the surface of the metal structure, enabling it to capture local structural response characteristics and maintain high energy conversion efficiency under low-frequency broadband vibrations. Wireless sensing nodes effectively balance energy consumption and communication load through CH aggregation and dynamic DC control, ensuring energy balance and data integrity across the entire network in a multi-node collaborative state. These results demonstrate that the proposed

system can not only operate stably on crawler cranes but also has the potential to be extended to other large-scale engineering equipment.

The piezoelectric model in this study is based on a linear relationship, but existing research has shown that nonlinear effects have a significant impact on energy harvesting under high amplitude or random excitation conditions (Zhao et al., 2025a). Therefore, future studies should explore the design of multi-stable energy harvesters, incorporating structures such as symmetrical stiffness and V-shaped arrays, to enhance energy conversion efficiency (Li et al., 2024). Furthermore, although this experiment used steady-state excitation, the actual operation of the crane involves non-stationary vibrations. Literature indicates that accelerated spectrum replay technology can effectively simulate the non-stationary vibration characteristics in real-world operations (Zhao et al., 2025b). Therefore, future research could introduce this technology to better simulate the actual working environment. Regarding node lifespan, while tests were conducted under specific conditions, considering that different environments and equipment may affect node performance, future work needs to further verify node lifespan under diverse environmental conditions. Lastly, future research will integrate multi-stable energy harvesters and biomimetic structure designs to further enhance the system's energy conversion efficiency and adaptability. These designs have demonstrated the potential to improve system stability and flexibility in other fields (Huang et al., 2025; Wang and Wang, 2024).

6 Conclusion

A self-powered system design based on PEH was proposed to address the wireless sensors for crawler cranes being difficult to be online for a long time due to energy supply bottlenecks. Firstly, a crane operating condition PEH model was established, combined with circuit topology design to improve energy conversion efficiency. A wireless sensor system integration solution was constructed, covering node layout, low-power communication protocols, and energy management strategies. The experiment showed that the output power of PEH was 8.0 mW at 0.5 g and 32 Hz, which was 47.5% higher than that of the unoptimized state. After joint optimization, the node lifespan was 397.4 h, with an increase of 65.6% compared to the unoptimized state. Moreover, the proportion of failed nodes after 500 h was only 25.2%, and the communication success rate remained above 90%. The joint optimization scheme increased throughput to 102.6 kbps and reduced latency to 65.3 ms. The results show that PEH and self-powered wireless sensor systems can improve the efficiency of crawler cranes. The system meets the maintenance free and long-term stable monitoring requirements of typical working conditions, providing a feasible solution for the efficient operation and intelligent monitoring of crawler cranes. However, the study only verifies single-node energy self-sufficiency, and multi-node energy routing and dynamic load balancing have not yet been analyzed. Future research will build a multi-node energy routing protocol based on energy mapping to achieve a distributed self-powered sensor network for the entire machine. Furthermore, extending this system to larger-scale engineering equipment such as cranes, fans, excavators, and port machinery requires addressing more demanding environmental conditions, including significantly different vibration spectrum distributions, temperature and humidity shocks, and dust and salt spray corrosion. The complex structure also leads to an increased number of sensor nodes, uneven energy distribution, and insufficient node energy. To address these challenges, future plans include developing a multi-node energy routing protocol. This protocol enables dynamic energy sharing and task scheduling among multiple vibration energy acquisition nodes, allowing the system to adaptively supply power based on local node energy conditions, vibration intensity, and service priorities. This will further improve the system's availability across different equipment, environments, and scales.

Data availability statement

The original contributions presented in the study are included in the article/supplementary material, further inquiries can be directed to the corresponding author.

Author contributions

YS: Writing – review and editing, Methodology, Writing – original draft, Investigation, Software. HL: Writing – original draft, Data curation, Writing – review and editing, Conceptualization.

Funding

The author(s) declared that financial support was not received for this work and/or its publication.

Conflict of interest

The author(s) declared that this work was conducted in the absence of any commercial or financial relationships that could be construed as a potential conflict of interest.

Generative AI statement

The author(s) declared that generative AI was not used in the creation of this manuscript.

Any alternative text (alt text) provided alongside figures in this article has been generated by Frontiers with the support of artificial intelligence and reasonable efforts have been made to ensure accuracy, including review by the authors wherever possible. If you identify any issues, please contact us.

Publisher's note

References

Amer, T. S., Bahnasy, T. A., Abosheiaha, H. F., Elameer, A. S., and Almahalawy, A. (2025). The stability analysis of a dynamical system equipped with a piezoelectric energy harvester device near resonance. *J. Low Freq. Noise, Vib. Act. Control* 44 (1), 382–410. doi:10.1177/14613484241277308

Baroiu, N., Păunoiu, V., Teodor, V. G., Moroşanu, G. A., and Crăciun, R. S. (2023). Aspects regarding the study of hydraulic and mechanical parameters of a "spider crane" system. *J. Eng. Stud. Res.* 29 (3), 27–38. doi:10.29081/jesr.v29i3.003

Bello, R. W., and Oladipo, M. A. (2024). Mask YOLOv7-based drone vision system for automated cattle detection and counting. *Artif. Intell. Appl.* 2 (2), 115–125. doi:10.47852/bonviewAIA42021603

Gupta, D., Ramesh, J. V. N., Kumar, M. K., Alghayadh, F. Y., Dodda, S. B., Ahanger, T. A., et al. (2024). Optimizing cluster head selection for e-commerce-enabled wireless sensor networks. *IEEE Trans. Consumer Electron.* 70 (1), 1640–1647. doi:10.1109/TCE.2024.3360513

Harle, S. M. (2024). Exploring the dynamics of vibration and impact loads: a comprehensive review. *Int. J. Struct. Eng.* 14 (1), 1–24. doi:10.1504/IJSTRUCTE.2024.136893

He, Q., and Briscoe, J. (2024). Piezoelectric energy harvester technologies: synthesis, mechanisms, and multifunctional applications. *ACS Appl. Mater. and Interfaces* 16 (23), 29491–29520. doi:10.1021/acsami.3c17037

Huang, X., Hua, X., and Chen, Z. (2025). Exploiting a novel magnetoelastic tunable bi-stable energy converter for vibration energy mitigation. *Nonlinear Dyn.* 113 (3), 2017–2043. doi:10.1007/s11071-024-10337-z

Kermani, M., Shirdare, E., Parise, G., Bongiorno, M., and Martirano, L. (2022). A comprehensive technoeconomic solution for demand control in ports: energy storage systems integration. *IEEE Trans. Industry Appl.* 58 (2), 1592–1601. doi:10.1109/TIA.2022.3145769

Kundu, L., Lin, X., and Gadiyar, R. (2025). Toward energy efficient RAN: from industry standards to trending practice. *IEEE Wirel. Commun.* 32 (1), 36–43. doi:10.1109/MWC.010.2400061

Lang, J., Yuan, M., Meng, Y., Tang, S., Zhang, B., Ke, Q., et al. (2025). Significantly enhanced transduction coefficient of PLZT ceramics to obtain a very high power density as a piezoelectric energy harvester. *ACS Appl. Mater. and Interfaces* 17 (2), 3560–3569. doi:10.1021/acsami.4c15196

Li, Z., Wang, C., Shen, F., Peng, Y., and Wang, M. (2024). *Goose queue inspired V-Array with cross-section variations for enhanced electromechanical energy harvesting behaviors*. IEEE/ASME Transactions on Mechatronics. doi:10.1109/TMECH.2024.3496935

Meisak, D., Plyushch, A., Kinka, M., Balčiūnas, S., Kalendra, V., Schaefer, S., et al. (2024). Effect of particle size on the origin of electromechanical response in BaTiO3/PDMS nanogenerators. *ACS Appl. Electron. Mater.* 6 (10), 7464–7474. doi:10.1021/acsaelm.4c01333

Mohsen, S., Zekry, A., Youssef, K., and Abouelatta, M. (2021). A self-powered wearable wireless sensor system powered by a hybrid energy harvester for healthcare applications. *Wirel. Personal. Commun.* 116 (4), 3143–3164. doi:10.1007/s11277-020-07840-y

Peng, Y., Wang, Y., Raffik, R., Jagota, V., Bhatia, K. K., Kumar, R., et al. (2022). Vibration state monitoring of mechanical equipment based on wireless sensor network technology. *Electrica* 22 (3), 428–437. doi:10.5152/electrica.2022.22051

Song, F., and Xiong, Y. (2022). Design of a piezoelectric–electromagnetic hybrid vibration energy harvester operating under ultra-low frequency excitation. *Microsyst. Technol.* 28 (8), 1785–1795. doi:10.1007/s00542-022-05332-6

Song, C., Liu, S., Han, G., Zeng, P., Yu, H., and Zheng, Q. (2022). Edge-intelligence-based condition monitoring of beam pumping units under heavy noise in industrial internet of things for industry 4.0. *IEEE Internet Things J.* 10 (4), 3037–3046. doi:10.1109/JIOT.2022.3141382

Tabak, A., Safaei, B., Memarzadeh, A., Arman, S., and Kizilors, C. (2024). An extensive review of piezoelectric energy-harvesting structures utilizing auxetic materials. *J. Vib. Eng. and Technol.* 12 (3), 3155–3192. doi:10.1007/s42417-023-01038-9

Wang, T., and Wang, H. (2024). Multistable pendulum wave energy harvesting under multidirectional irregular excitations. *IEEE/ASME Trans. Mechatronics* 29 (4), 3175–3183. doi:10.1109/TMECH.2024.3400989

Zhang, Q., Xin, C., Shen, F., Gong, Y., Zi, Y., Guo, H., et al. (2022). Human body IoT systems based on the triboelectrification effect: energy harvesting, sensing, interfacing and communication. *Energy and Environ. Sci.* 15 (9), 3688–3721. doi:10.1039/D2EE01590K

Zhang, X., Huang, X., and Wang, B. (2024). A quad-stable nonlinear piezoelectric energy harvester with piecewise stiffness for broadband energy harvesting. *Nonlinear Dyn.* 112 (22), 19633–19652. doi:10.1007/s11071-024-10077-0

Zhao, L., Gong, Y., Shen, F., Peng, Y., Xie, S., and Li, Z. (2025a). Diminishing potential well barrier in bi-stable energy harvesters by introducing symmetric stiffness. *Thin-Walled Struct.* 209, 112880. doi:10.1016/j.tws.2024.112880

Zhao, L., Gong, Y., Shen, F., Wu, H., Peng, Y., Xie, S., et al. (2025b). Effect of stability state transition of variable potential well in tri-hybridized energy harvesters. *Mech. Syst. Signal Process.* 223, 111855. doi:10.1016/j.ymssp.2024.111855

Zou, Y., Bo, L., and Li, Z. (2021). Recent progress in human body energy harvesting for smart bioelectronic system. *Fundam. Res.* 1 (3), 364–382. doi:10.1016/j.fmre.2021.05.002